Advanced Steel Construction – Vol. 22 No. 1 (2026) 48–63
DOI:10.18057/IJASC.2026.22.1.5

ANALYTICAL AND NUMERICAL INVESTIGATION OF ULTRA-HIGH-PERFORMANCE CIRCULAR CONCRETE-FILLED DOUBLE-TUBES UNDER FIRE CONDITIONS

Mohamed Ghannam [1], Sameh Lotfy [2], A.H.A. Abdelrahman [1, *], Mohammad AlHamaydeh [3] and Md Kamrul Hassan [4]

[1] *Structural Engineering Department, Faculty of Engineering, Mansoura University, Egypt*
[2] *Civil Engineering Department, MISR Higher Institute for Engineering and Technology, Mansoura, Egypt*
[3] *Department of Civil Engineering, American University of Sharjah, PO Box 26666, Sharjah, United Arab Emirates,*
[4] *Lecturer in Fire Safety Engineering, School of Engineering, Design and Built Environment, Western Sydney University, Penrith, NSW 2751, Australia*
** (Corresponding author: E-mail: a_hussain@mans.edu.eg)*

ABSTRACT

This study presents an analytical and numerical investigation of ultra-high-performance concrete-filled double-skin tubular (UHPC-CFDST) columns with circular cross-sections under fire conditions. An automated algorithm was employed to develop and verify a finite element (FE) model capable of accurately simulating CFDST columns incorporating different concrete types (normal concrete, ultra-high-performance concrete (UHPC), and lightweight concrete) in both core and ring regions. The validated model was used to examine the influence of key parameters, offering deeper insight into the behavior of such columns under fire. Three temperature-dependent material models were developed to represent UHPC, lightweight concrete, and high-strength steel at elevated temperatures. Additionally, a finite difference-based thermal model was proposed to simulate the temperature distribution across the column cross-section and to predict fire resistance (FR) time. To the best of the authors' knowledge, existing fire design standards do not provide specific models for CFDST columns under fire, and available research in this area is limited. This study addresses this gap by evaluating the applicability of Eurocode 4 (EC4) and proposing a simplified modification that improves the prediction accuracy of fire resistance for UHPC-CFDST columns.

ARTICLE HISTORY

Received: 18 July 2025
Revised: 29 September 2025
Accepted: 5 October 2025

KEYWORDS

Concrete-filled double- tubes;
Ultra-high-performance concrete;
Analytical model;
Numerical model;
Fire standards;
Axial load capacity;
Fire resistance

1. Introduction

Concrete-filled double-skin tubular (CFDST) columns were first introduced in 1989 [1], and since then, they have gained significant attention from researchers and increasing popularity in the construction industry due to their advantages over conventional concrete-filled steel tube (CFST) columns. These advantages include higher strength, lighter structural weight with improved ductility, better fire performance, and enhanced cyclic behavior [1-8].

A CFDST column consists of two concentric steel tubes, with the annular gap between them filled with concrete, while the core remains hollow. When the hollow core is also filled with concrete, the system is referred to as a concrete-filled double tube (CFDT) column. Various parameters influencing the behavior of CFDST and CFDT columns have been studied, including the nominal steel ratio (α_n), the hollow ratio (χ) defined for CFDST columns as $\chi = D_i/(D_O\text{-}2t_O)$, the concrete compressive strength (f_c'), the yield strength of the outer and inner steel tubes ($f_{syo,}$ and f_{syi} respectively), and the diameter-to-thickness ratio (D/t) for both tubes [3, 9-11].

The interaction between steel tubes and the concrete ring in CFDST columns has been investigated by Tao *et al.* [3] and Huang *et al.* [11]. At the initial loading stage, no interaction occurs between the outer tube and the concrete ring due to the difference in Poisson's ratio between steel and concrete. However, as axial loading increases, the resulting lateral strain leads to contact and interaction between the two materials. A different behavior is observed between the inner tube and the concrete ring: interaction occurs early in the loading process due to the higher lateral strain of the steel tube compared to the concrete. As the concrete enters the elastic-plastic stage, this interaction gradually diminishes.

When the peak load is reached, contact is formed again between concrete ring and inner tube as a result of larger lateral strain of concrete compared to steel due to cracks formation of in concrete ring [3, 11]. Huang *et al.* [11] found numerically that load axial capacity decreased by 15% and 26 % for square and circular columns, respectively as the hollow ratio increased from zero to 0.75. It was found that the effect of hollow ratio on concrete stress is more significant in circular columns compared to square ones. However, column ductility is not affected [3, 11].

From the FE model analysis that was proposed by Huang *et al.* [11] it was found that, the axial Load capacity of stub CFDST columns increases by about 71% due to an increase in concrete strength from 30 MPa to 90 MPa. When the steel yield strength of the outer tube increased by approximately 79 %, the axial load capacity increased by about 30%. When the nominal steel ratio increased by 3 times, the axial capacity increased by 62 and 72 % for square and circular columns, respectively. From the research done previously [3, 10, 11], it was found that, inner tube yield strength, and width-to-thickness ratio have no significant effect on the axial capacity of stub CFDST columns because of the small steel area on the inner tube compared to the outer tube, the main role of inner tube is confining the concrete ring. The inner tube width-to-thickness ratio affects the failure mode of the inner tube.

CFDT columns have many advantages that overcome the conventional CFST and CFDST columns. Compared to CFDST columns, filling the central void with concrete (CFDT columns) improves load capacity and reduces inner tube buckling [12]. A key advantage of CFDT columns that overcome both CFST and CFDT columns is their high fire resistance [2, 13, 14], as the outer concret ring protect the inner steel tube from temperature development during fire, Besides, CFDT columns provide more load capacity compred to CFST and CFDST columns as a result of the pressence of inner concrete core which is not available in CFDST columns and inner steel tube which is not availale in CFST columns.

Lu *et al.* [15] provide some design guidelines for CFDST columns in fire. Increasing yield strength and/or thickness of the inner tube and decreasing the yield strength and/or thickness of the outer tube help in improving the fire resistance. A similar finding was obtained by Romero *et al.* [2]; drain holes in the outer tube are beneficial as they help to release the water vapor pressure. The minimum thickness of the concrete ring is 50 mm, using steel fiber in concrete help in increasing the fire resistance. Xiong [16] could not decide which has better fire performance CFST columns or CFDST columns

Some researchers provide design models for CFDST columns in fire [17-21]. Yao *et al.* [22] presented a design model based on the Rankine approach for columns subjected to uniform temperature, while Yao *et al.* [23] used the Rankine approach for non-uniform heating. [15] present fire design tables. Some researchers tried to improve the fire performance of CFDST columns. Jia-qi *et al.* [13] found that using stainless steel in the outer tube increases the fire resistance compared with using carbon steel. Shekastehband *et al.* [24] used found that using stiffeners with the inner tube and outer tube can increase the fire resistance of the CFDST column significantly as the stiffener in the outer tube absorbs more heat, allowing the outer tube to withstand applied load for a longer time beside stiffeners increase the contact between steel tube and concrete core and reduce buckling of steel tubes this was also concluded at ambient temperature [9]. Zhu *et al.* [19], Zhu *et al.* [20]and Zhu *et al.* [21]

presented a design model for circular CFDT columns under axial and eccentric load based on Eurocode 4 [25] design procedures.

Using HSC and UHPC is considered a modern method to improve the fire performance of CFDST and CFDT columns. Ultra-high performance concrete (UHPC) has been increasingly used nowadays due to its advantages, such as high strength, high fracture capacity, and high durability. Using ultra-high performance concrete (UHPC) in CFDST and CFDT columns has a dual benefit; from one side, UHPC will lead to increased CFDT column capacity; from another side, steel tubes will help in overcoming one of the main disadvantages of UHPC which is brittleness by providing more ductility to the column. Also steel tube will help in increasing column capacity by the confinement that will be provided to the concrete [26].

Many researches have been conducted to investigate the fire behaviour of UHPC as it has been considered as a relatively new construction material [27-34]. Banerji and Kodur [31] and Xiong and Liew [35] found that compressive strength and elastic modulus of UHPC are reduced in a higher rate compared to reduction occurred in normal strength concrete (NSC) at elevated temperatures. However, Banerji and Kodur [31] found that the presence of steel fibers helps in reducing the degradation in tensile strength and ductility in UHPC compared to conventional concrete. Many researchers find the addition of polypropylene fibers to UHPC reduces significantly concrete spalling [34, 36, 37], which is explained as a result of the melting of polypropylene at high temperatures which maintains internal vapor pressure and prevents explosive spalling.

Xiong and Liew [38] found that using NSC and UHPC give similar fire performance for CFST columns, however using Ultra High Strength Concrete (UHSC) gives higher fire resistance compared with using NSC and HSC. A similar finding was obtained by Xiong and Liew [39]. Xiong and Liew [39] found that using buckling curve “d” in Eurocode simplified model and M-N interaction diagram give a good prediction for the fire resistance of CFST column. However, the M-N interaction diagram gives better predictions in cases of high load lever (especially > 0.65). Wang *et al.* [40] found that increasing the steel fiber and course aggregates can significantly increase the fire resistance of the CFST column filled with UHPC. Wang *et al.* [40] proposed a design model for CFST column filled with UHPC.

Romero *et al.* [2] found that using UHPC in the core of CFDT columns may give lower fire resistance compared to NSC. This is because the load level was kept constant and, so the load value applied on the UHPC column was bigger than the NSC columns. In slender columns, the concrete core do not have a significant effect on column capacities. However, its main role is participating in the column stiffness and preventing inner tube buckling and reducing the temperature in the inner tube, also, in the same study, it was found that Eurocode 4 gives unsafe prediction for the fire resistance of CFDT columns.

Camargo *et al.* [41] and Lopes and Rodrigues [14] presented studies on restrained CFDT columns with HPC for circular and square columns, respectively. The results show that HSC do not have a significant effect in increasing the critical time but can increase the failure time for restrained square columns. Besides, the study shows that the available design codes are insufficient for designing these types of columns.

Although extensive research has been conducted on the fire behavior of concrete-filled steel tube (CFST) columns, studies on the fire performance of CFDST and CFDT columns filled with high-strength concrete (HSC) or ultra-high-performance concrete (UHPC) remain limited [2, 14, 41]. To the best of the authors’ knowledge, current fire design standards do not provide a design model for CFDST columns incorporating UHPC. This study aims to address this research gap through analytical and numerical investigations of ultra-high-performance concrete-filled double-skin tubular (CFDST) columns under fire.

Three material models were developed using existing experimental data for UHPC, lightweight concrete (LWC), and high-strength steel at elevated temperatures. An automated algorithm was employed to develop a verified finite element (FE) model that accurately simulates circular CFDST columns with different concrete types—normal concrete, LWC, and UHPC—in the core and ring regions. The validated FE model was then used to perform a parametric study to better understand the behavior of these columns under fire conditions.

In addition, a finite difference (FD) model was developed in MATLAB to simulate the temperature distribution across the cross-section and predict fire resistance based on Eurocode 4, Part 1.2. A simplified analytical model based on EC4 Part 1.2 is also proposed to estimate the axial load capacity and fire resistance of CFDST columns under various fire exposure scenarios.

2. Material properties at elevated temperature

This section is divided into two subsections. The first subsection compiles available experimental data on the mechanical properties of ultra-high-performance concrete (UHPC) at elevated temperatures. The second subsection reviews the thermal and mechanical properties of high-strength steel under elevated temperature conditions.

2.1. Mechanical properties of UHPC under fire

In the literature, three types of material fire tests are commonly reported: stressed, unstressed, and residual conditions. In residual conditions, specimens are heated to a target temperature, maintained until a uniform temperature is achieved throughout the section, then cooled before being loaded to failure. In unstressed conditions, specimens are similarly heated and held at a constant temperature, but are loaded to failure without cooling. Stressed conditions are similar to unstressed ones, except that a predetermined load is applied during the heating process [31]. Residual testing is simpler to conduct and is suitable for evaluating material properties in the post-fire stage, whereas unstressed testing is more appropriate for assessing properties during fire exposure, which is the focus of this paper. Accordingly, the collected data for HSC and UHPC under fire are limited to unstressed conditions, as listed in Table 1. Previous studies have shown that concrete strength does not significantly influence thermal expansion [42]. The data set in this section will be used to propose the material model for UHPC at elevated temperature in section 4.2.

Table 1
Details of recent fire test on HSC and UHPC at elevated temperature

Ref.	Specimens shape (mm)	Specimens size (mm)	Temperature limit (^{O}C)	*fc*’ (MPa)
Xiong [16] and Xiong and Liew [35]	Cylinder	100X200	800	166.6
Banerji and Kodur [31]	Cylinder	75X150	750	171 and 177
Choe *et al.* [43]	Cylinder	100X200	700	100,150 and 200
Lee *et al.* [42]	Cylinder	100X200	700	83, 134.8 and 184.5
Khaliq [44]	Cylinder	100X200	800	64 and 72
Cheng *et al.* [45]	Cylinder	100X200	800	79, 78.3, 81.4 and 85.5
Phan and Carino [46]	Cylinder	100X200	450	98.2, 81.2, and 72.3

2.2. Mechanical properties of high strength steel at elevated temperatures

Two main types of experiments are used to assess the mechanical behavior of steel coupons at elevated temperatures: steady-state tests and transient-state tests. In the transient test, a tensile load is applied while the temperature is gradually increased until failure occurs. In contrast, the steady-state test involves heating the coupons to a target temperature, maintaining it for a period to ensure uniform distribution, and then applying the tensile load until failure. Due to its relative simplicity, the steady-state method is more commonly adopted in experimental research. In this study, the most recent steady-state test data available for high-strength steel are compiled, as shown in Table 2. The data set in this section will be used to propose the material model for high strength steel at elevated temperature in section 4.2.

3. Previous experimental fire tests on CFDST Columns

This section summarizes available fire resistance tests conducted on CFST columns filled with UHPC, as well as CFDT and CFDST columns filled with either UHPC or NSC. Table 3 presents the collected data, where D_o and D_i are the outer and inner tube diameters, t_o and t_i are the corresponding wall thicknesses, f_{yo} and f_{yi} represent the yield strengths of the outer and inner tubes, and f'_{co} *and* f'_{ci} are the cylinder compressive strengths of the concrete ring and core, respectively. L denotes the column length, n is the load ratio, and FR is the fire resistance duration in minutes. This experimental database will be used in the parametric study and to validate the finite element (FE) model. The data set in table 3 shows the limitation of available test result on CFDT column under elevated temperature.

Table 2
Collected fire test on high strength steel at elevated temperature

Ref.	Temperature limit (^{O}C)	*Fy* (MPa)
Chen *et al.* [47]	940	789
Lange and Wohlfeil [48]	900	431.5, 445.6
Qiang *et al.* [49]	700	690
Qiang *et al.* [50]	700	460
Choi *et al.* [51]	900	701
Heidarpour *et al.* [52]	600	1283, 1331
Wang *et al.* [53]	900	965
Li and Song [54]	800	780

Table 3
Summary of test data of CFDST and CFST (with UHPC) members under fire

Shape	Ref.	No. of specimens	D_o/D_i (mm)	t_o/t_i (mm)	L (mm)	f'_{co}/f'_{ci} MPa	f_{yo}/f_{yi} MPa	n	FR min
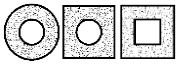	[55]	6	280-300 / 140-225	5/5	3810	38 cu	320/320	0.32-0.65	40-240
	[2]	6	200/114	3-6/8-3	3180	30/150	232-407/329-512	0.2	33-104
	[56]	12	101-127/50-76	3-4	600	38-41 fcu	597-430/762-449	Residual strength	60-90
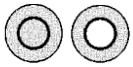	[17]	6	325/219-159	6/6	3800	46.8 fcu	295-255/285-260	0.4-0.6	68-17
	[16]	6	219-200/114-100	16-12/6.3-8	3810	172-163	432-785/468-825	0.33-0.95	15-25
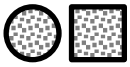	[16]	16	200-273	16-10	3810	161-181	418-785	0.34-0.88	18-192

4. Finite element modelling

4.1. General

A Finite element (FE) program, ABAQUS [57] was used to develop the FE model for CFDST columns. The inner and the outer steel tubes were modelled using an S4R shell element with 4 nodes having six degrees of freedom for each node. The inner and outer concrete core was modelled using 8 node C3D8R solid element with 3 degrees of freedom for each node.

A sequential-coupled thermal stress analysis was performed to simulate the fire behavior of CFDST columns. First, a thermal analysis was performed to simulate the temperature development within the column cross-section during the fire, and then the temperature development through the cross-section during the fire was imported into the stress analysis through a predefined field in the stress analysis. The meshing size in the thermal and the stress analysis was identical. Thermal analysis was performed as previously established by the authors [58]. The Finite element (FE) model is presented in Fig. 1.

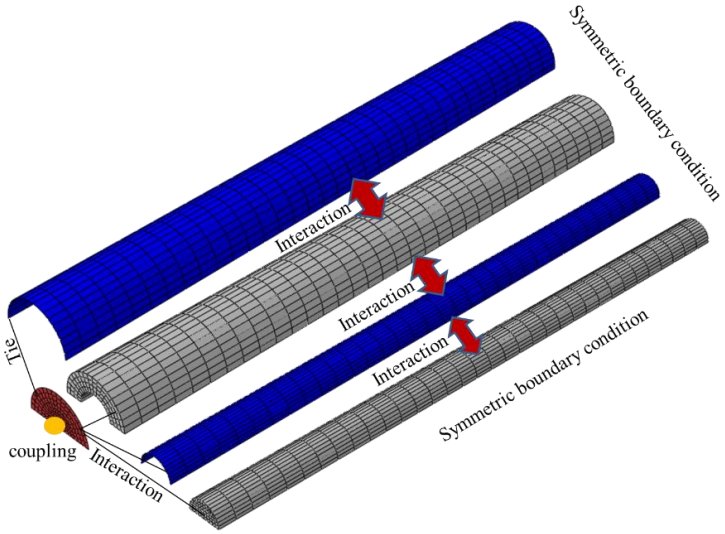

Fig. 1 Finite element model

4.2. Material properties

Eurocode 3 [59] was adopted for modeling the mechanical behavior of both the inner and outer steel tubes. For concrete material modeling, the Concrete Damage Plasticity (CDP) model was employed, with plasticity parameters and fracture energy defined according to the recommendations by Liu *et al.* [60]. The behavior of normal-strength concrete (NSC) in both the outer ring and inner core was modeled using Eurocode 2 [61] , with the tensile stress behavior defined by the CEB-FIB model [62].

For ultra-high-performance concrete (UHPC), a new temperature-dependent strength reduction model was developed based on experimental data reported in previous studies [25, 42, 57, 63]. The adopted stress–strain relationship followed the model proposed by Lie and Irwin [64]. Additionally, a new thermal expansion model for UHPC was proposed, derived from experimental results reported by Lee *et al.* [42]. The proposed strength reduction factor, thermal expansion, and modulus of elasticity reduction factor are illustrated in Fig. 2 (a, b, and c), and are defined by Eqs. (1–3).

The reduction factor for compressive strength is shown in the next equation

$$\begin{cases} 1.0 & T = 20 \\ -3.21x10^{-3}T + 1.0642 & 20 < T \le 100 \\ 1.1679x10^{-3}T + 0.6263 & 100 < T \le 200 \\ 4.157x10^{-9}\,T^3 - 6.584x10^{-6}\,T^2 + 2.075x10^{-3}\,T + 0.675 & 200 < T < 1000 \end{cases} \quad (1)$$

Thermal expansion is shown in the next equation

$$\begin{cases} \left[\frac{1}{342.233-0.5044T+45423.8860/T} - 0.0004\right] / (T-20) & 20 < T \le 625 \\ 0.0097/(T-20) & T > 625 \end{cases} \quad (2)$$

The reduction factor for the modulus of elasticity is shown in the next equation

$$\begin{cases} 1 & T = 20 \\ 1.267x10^{-6}\,T^2 - 2.279x10^{-3}\,T + 1.04 & 20 < T < 1000 \end{cases} \quad (3)$$

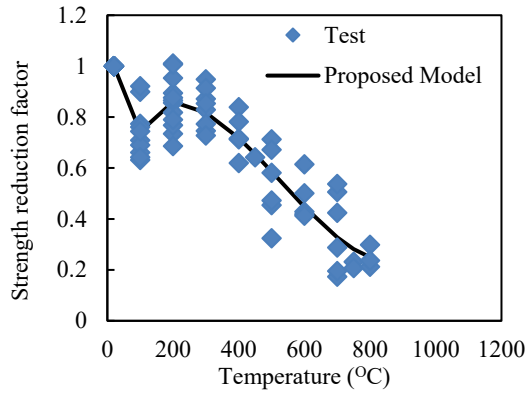

(a) Strength reduction factor

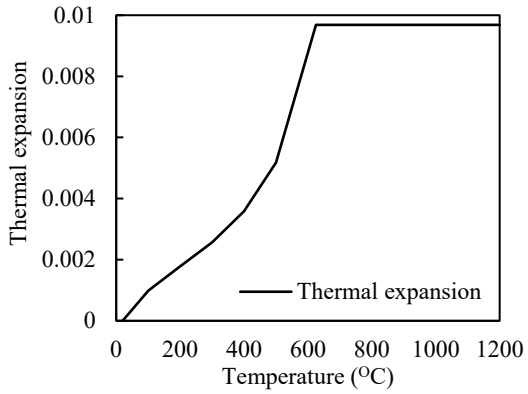

(b) Thermal expansion

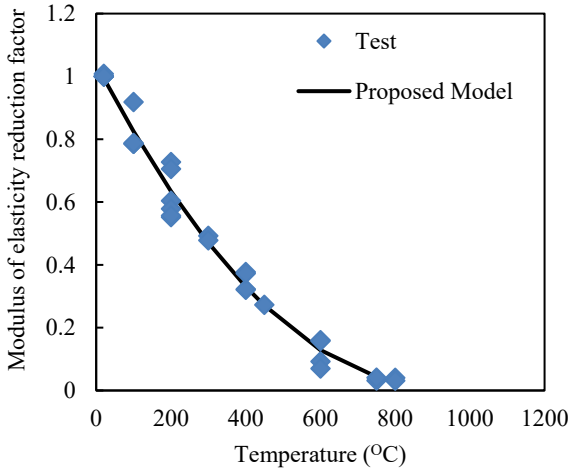

(c) Modulus of elasticity reduction factor

Fig. 2 proposed model for UHPC

A temperature-dependent material model was also developed for lightweight concrete (LWC), based on previously published experimental data [58, 59, 61, 65] and the compressive stress–strain relationship specified in [66].

The proposed model is illustrated in Fig. 3, and its mathematical formulation is defined by Eqs. (4–8).

The reduction factor for compressive strength is shown in the next equation

$$\begin{cases} 1.0 & T = 20 \\ \dfrac{0.5672}{1.0 + 0.0197 * \mathrm{EXP}(0.0089 * \mathrm{T})} + 0.434 & 20 < T \leq 800 \end{cases} \quad (4)$$

The peak strain value is shown in the next equation

$$\begin{cases} 0.0025 & T = 20 \\ 0.0025 \times (0.9915 + 2.653 \times 10^{-5} \times T^2 - 1.598 \times 10^{-6} \times T^{2.5} + 2.7389 \times 10^{-8} \times T^3) & 20 < T \leq 800 \end{cases} \quad (5)$$

The reduction factor for the modulus of elasticity is shown in the next equation

$$\begin{cases} 1.0 & T = 20 \\ 0.6518 + 0.0014 \times T - 0.123T^{0.5} + 0.2907 \ln(T) & 20 < T \leq 800 \end{cases} \quad (6)$$

The reduction factor for tensile strength is shown in the next equation

$$\begin{cases} 1.0 & T = 20 \\ 0.8897 - 0.0019T - 2.0174 \times 10^{-10} \times T^3 + 0.0333T^{0.5} & 20 < T \leq 800 \end{cases} \quad (7)$$

Thermal expansion is shown in the next equation

$$\begin{cases} 9.1 \times 10^{-6} & T = 20 \\ 9.2676 \times 10^{-6} - \dfrac{6.1894 \times 10^{-4}}{T} + \dfrac{0.0896}{T^2} - \dfrac{2.06981927}{T^3} & 20 < T \leq 800 \end{cases} \quad (8)$$

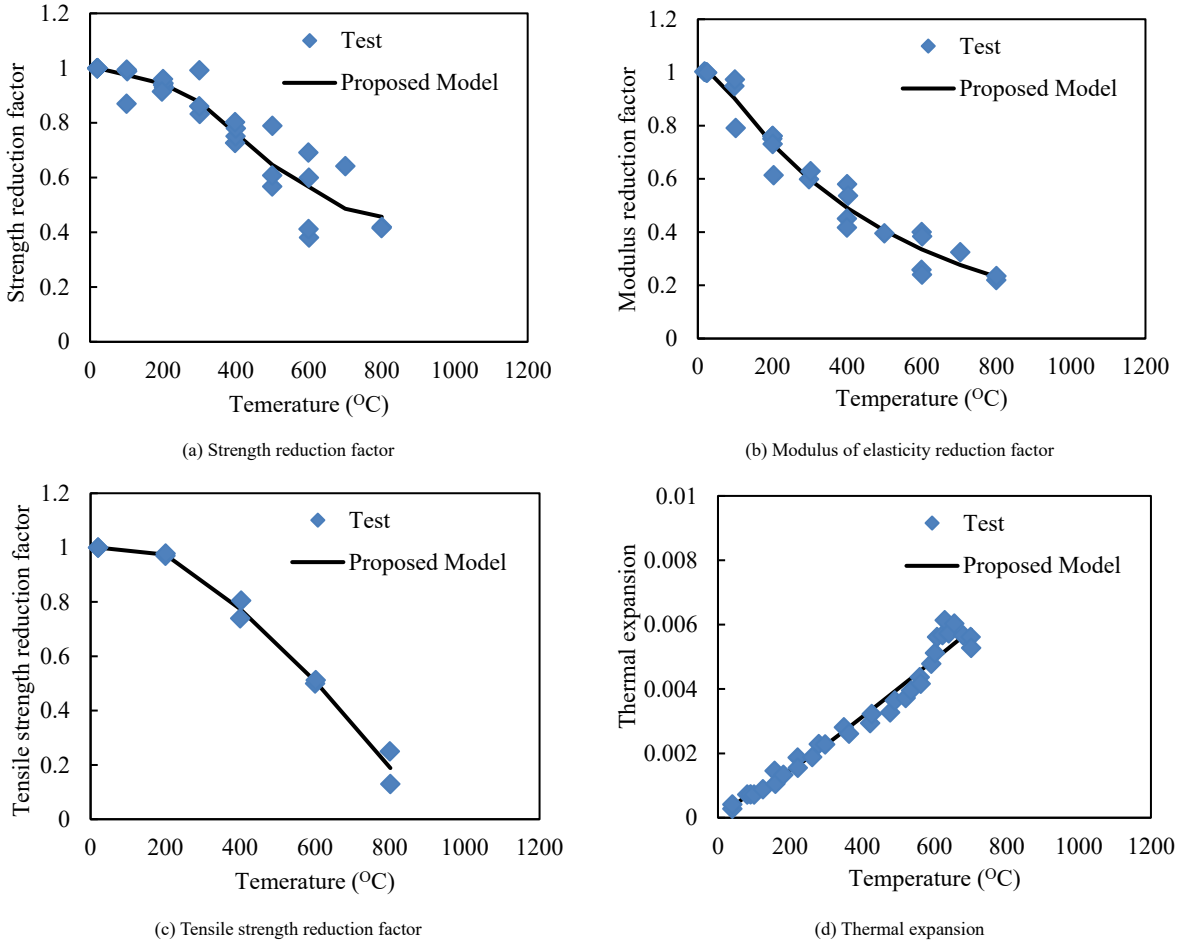

(a) Strength reduction factor

(b) Modulus of elasticity reduction factor

(c) Tensile strength reduction factor

(d) Thermal expansion

Fig. 3 Proposed model for LWC

Tables 4 and 5 present a comparison between the results obtained from the proposed model and those from existing standards, evaluated against experimental data for UHPC and LWC, respectively. The standards included in the comparison are: Eurocode 2 (EC2) [61], Eurocode 4 (EC4) [25], he Koudr model for ultra-high-performance concrete [31], ACI [67], AISC [68], Australian standards [69] and ASCE [70].

According to EC2, concrete is categorized into four classes: NSC, Class 1, Class 2, and Class 3. NSC is further divided based on the type of coarse aggregate, either carbonate (calcareous) or siliceous, which are referred to in Table 4 as Euro_Car and Euro_Sili, respectively. Both Euro_Car and Euro_Sili correspond to concrete with a maximum cylinder compressive strength of 50 MPa. High-strength concrete in EC2 is divided into three categories: Class 1 (up to 60 MPa), Class 2 (up to 80 MPa), and Class 3 (up to 90 MPa), which are referred to in Table 4 as Euro_Class1, Euro_Class2, and Euro_Class3, respectively.

The results indicate that the proposed model provides the most accurate predictions when compared to the existing standards and codes.

Table 4
Evaluation for the proposed mode of UHPC

	Test/ Euro_car	Test/ Euro_sili	Test/ Euro _class1	Test/ Euro _class2	Test/ Euro _class3	Test/ Kodur [31]	Test/ AISC	Test/ AS/NZ 2327	Test/ ASCE	Test/ Proposed model
Compressive strength										
Mean	0.853	0.979	1.000	1.071	1.357	1.051	0.984	0.869	0.841	1.000
COV	0.197	0.264	0.248	0.225	0.319	0.215	0.233	0.222	0.256	0.182
Modulus of elasticity										
Mean	1.375	1.302	-	-	-	0.993	0.843	0.761	1.302	1.004
COV	0.264	0.282	-	-	-	0.161	0.178	0.223	0.282	0.164

Table 5
Evaluation of the proposed model of LWC

	Test/EC4	Test/AISC	Test/AS/NZ2327	Test/ASCE	Test/ACI216R-89	Test/Proposed model
Compressive strength						
Mean	1.100	1.100	1.172	1.100	1.134	1.016
COV	0.172	0.158	0.225	0.254	0.183	0.128
Modulus of elasticity						
Mean	-	0.819	0.944	-	0.971	1.014
COV	-	0.346	0.370	-	0.158	0.127
Thermal expansion						
Mean	-	-	-	-	0.983	1.010
COV	-	-	-	-	0.118	0.101

A third model was proposed to describe the material behavior of high-strength steel (HSS) at elevated temperatures. This model was developed using previous test results ([47-54]) and aims to provide reduction factors for strength and elastic modulus, following the stress–strain formulation introduced by Wang *et al.* [53]. Verification of the proposed model against experimental data is presented in Fig. 4, while comparisons with existing codes and standards are provided in Table 6. The proposed model for lightweight concrete (LWC) is detailed in Eqs. (9-10).

The reduction factor for yielding proof strength is shown in the next equation

$$\begin{cases} 1.0 & 20 \le T \le 200 \\ 0.030 + 0.9522 \times EXP(-9.4163 \times 10^{-13} \times T^{4.2949}) & 200 < T \le 1000 \end{cases} \quad (9)$$

$$\begin{cases} 1.0 & 20 \le T \le 200 \\ \dfrac{1.0126 + 3.3205 \times 10^{-13} \times T}{1.0 - 2.8338 \times 10^{-4} \times T^{4.4408}} & 200 < T \le 1000 \end{cases} \quad (10)$$

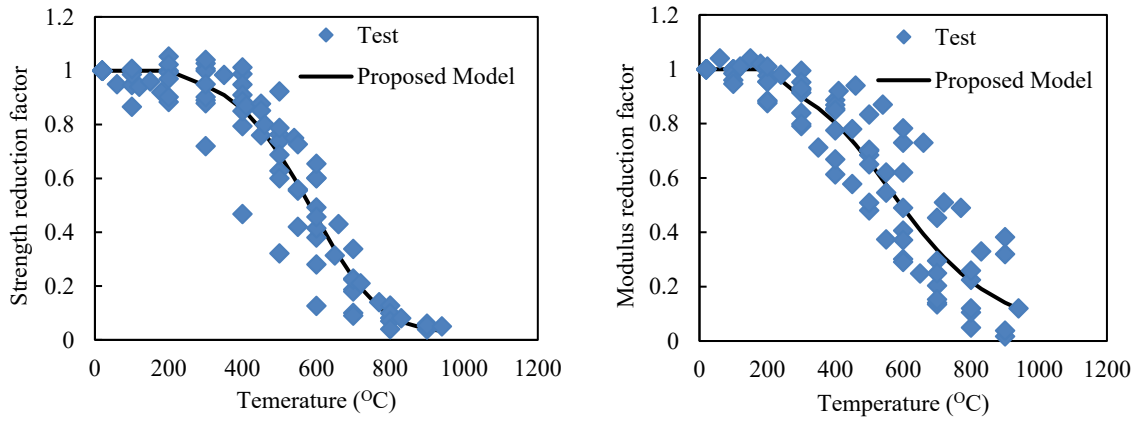

(a) Strength reduction factor (b) Modulus of elasticity reduction factor

Fig. 4 proposed model for HSS

Table 6
Evaluation of the proposed model for HSS

	Test/EC3	Test/ASCE	Test/AISC	Test/AS/NZ	Test/Proposed model
			Yield strength		
Mean	0.920	1.398	0.906	1.197	1.003
COV	0.221	0.325	0.222	0.378	0.223
			Modulus of elasticity		
Mean	1.485	1.698	1.428	2.191	1.012
COV	0.834	0.684	0.758	1.048	0.384

Based on the previous figures and tables, the proposed material models for UHPC, LWC, and high-strength steel demonstrate better agreement with test results compared to existing codes and models.

4.3. Interaction between steel tubes and concrete

Contact interaction was defined between the inner surface of the inner steel tube and the outer surface of the inner concrete core and between the outer surface of the inner steel tube and inner surface of the outer concrete core and between the inner surface of the outer steel tube and the outer surface of the outer concrete core. The contact interaction has a tangential behavior with a friction coefficient of 0.25 and a hard contact as normal behavior, which allow separation after contact.

4.4. Initial imperfections

Initial imperfection was introduced to the stress analysis through a separate pre-buckling analysis and using the 1st mode of buckling as an initial condition stress analysis with a maximum amplitude of L/1000 [71, 72].

4.5. Verification of finite element model

Limited experimental studies have investigated the fire behavior of concrete-filled double-skin tubular (CFDST) columns incorporating ultra-high-performance concrete (UHPC) or ultra-high-strength concrete (UHSC). In this study, finite element (FE) model verification was conducted using test results reported by Romero *et al.* [2]. Their experimental program involved testing twelve circular CFDST columns: six specimens under ambient conditions and six under elevated temperatures. The fire tests followed the ISO 834 standard fire curve [73]. All specimens were hinged, with a total column length of 3315 mm and an effective heated length of 3036 mm.

The specimen dimensions and material properties used in the experimental program are summarized in Table 7. The table also presents the fire resistance (FR) times obtained experimentally (FR_test) and those predicted by the proposed FE model (FR_FE). The average ratio of test-to-predicted fire resistance is 0.97, indicating good agreement between the experimental and numerical results.

Fig. 5 compares the displacement–time response from the test with that of the FE simulation, showing close correlation. Minor discrepancies can be attributed to initial geometric imperfections observed in the test specimens and the actual furnace temperature variations, which were not explicitly reported—only that the ISO 834 curve was followed. The verified FE model and the proposed temperature-dependent material models will be employed in the subsequent parametric study.

Table 7
Specimens details [2]

Spec. Name	D_{outer}	t_{outer}	D_{inner}	t_{inner}	Fy_{outer}	fc'_{outer}	Fy_{inner}	fc'_{inner}	N-applied	FR_test	FR_FE	FR Test / FE
C200-3-30-C114-8-00	200	3	114.3	8	300	46	377	0	283	76	77.68	1.02
C200-3-30-C114-8-30	200	3	114.3	8	332	46	403	45	325	104	105.4	1.01
C200-3-30-C114-8-150	200	3	114.3	8	272	44	414	136	355	98	84.75	0.86
C200-6-30-C114-3-00	200	6	114.3	3	407	43	343	0	329	48	41.08	0.86
C200-6-30-C114-3-30	200	6	114.3	3	377	44	329	42	392	45	40.81	0.91
C200-6-30-C114-3-150	200	6	114.3	3	386	43	343	126	415	33	38.7	1.17

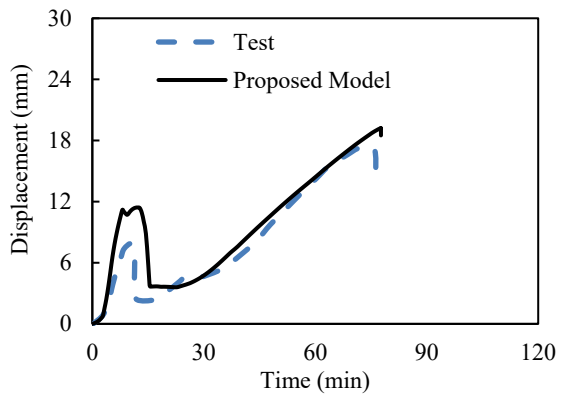

(a) C200-3-30-C114-8-00

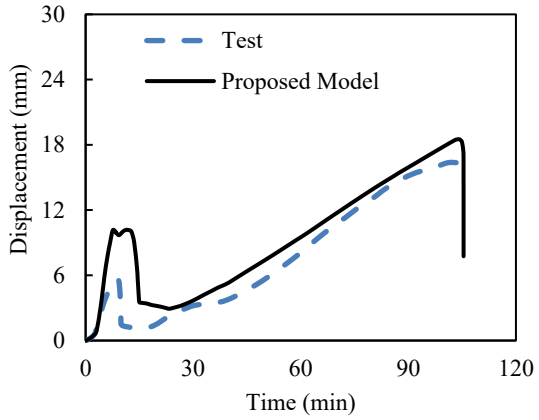

(b) C200-3-30-C114-8-30

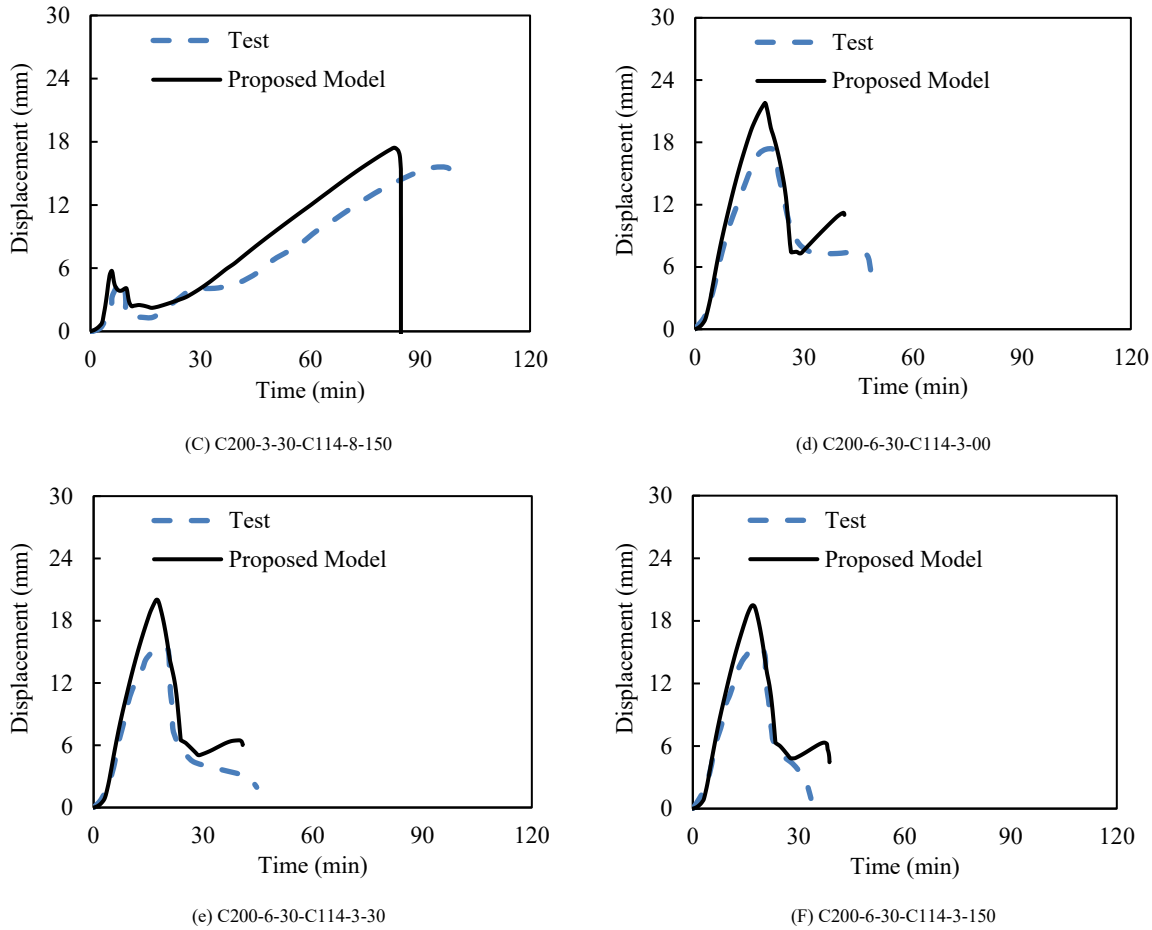

(C) C200-3-30-C114-8-150

(d) C200-6-30-C114-3-00

(e) C200-6-30-C114-3-30

(F) C200-6-30-C114-3-150

Fig. 5 Verification of the FE model

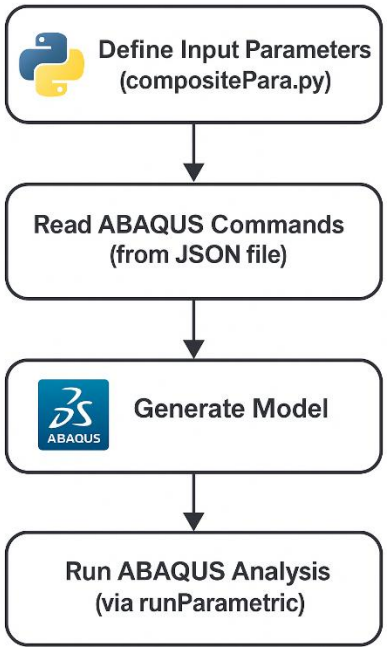

Fig. 6 Automated Finite Element Modeling Workflow for CFDT Columns Using Python and ABAQUS

4.6. Automated FE model

An automated finite element (FE) modeling framework was developed using the Python programming language. This framework allows users to define all column input parameters directly within the Python environment. The model is then automatically generated, executed in ABAQUS, and the simulation results are extracted without the need for manual intervention.

This automated approach offers significant benefits for both engineers who are not familiar with ABAQUS and researchers conducting extensive parametric studies. It streamlines the modeling process, reduces human error, and significantly saves time by automating model creation, execution, and post-processing.

Fig. 6 illustrates the workflow of the Python script. The user provides the input parameters through the compositePara file. ABAQUS-specific commands are parsed from a structured JSON file, and the model is then executed using the runParametric module.

5. Parametric studies

This section presents the results and discussion of the parametric study. The control column has an outer diameter of 500 mm with a 5 mm wall thickness, and an inner tube diameter of 300 mm with a thickness of 3 mm. The column is filled with ultra-high-performance concrete (UHPC) with a compressive strength of 120 MPa, and the steel has a yield strength of 360 MPa.

Fig. 7 illustrates the load distribution among the different components of the column during fire exposure. Fig. 7a presents the load distribution ratio of each component relative to the total applied load, while Fig. 7b shows the ratio relative to the initial applied load at the onset of fire exposure. The column undergoes several distinct stages before failure. Initially, the outer steel tube expands and carries the majority of the load. As its temperature increases, material degradation occurs, leading to a reduction in its load-carrying capacity. It eventually contracts until the loading plate contacts the outer concrete ring. Due to the high temperature, the outer concrete expands and begins to carry a significant portion of the load, more so than the inner steel tube and concrete core. As the outer concrete degrades, the inner steel tube and concrete core take on a greater share of the load. The inner steel tube, owing to its higher thermal expansion, carries more load than the concrete core until it also deteriorates. Ultimately, the inner concrete core becomes the sole load-bearing component until it too fails due to material degradation and excessive load.

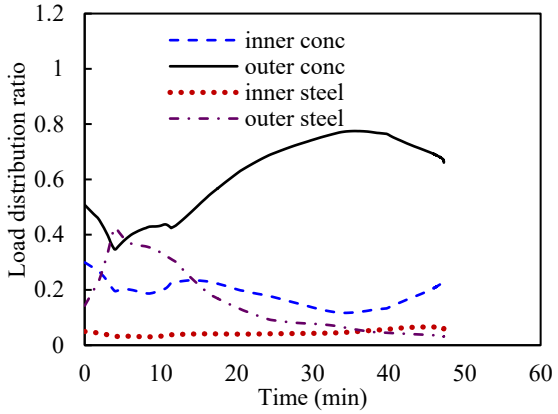

a) Ratio with total applied load

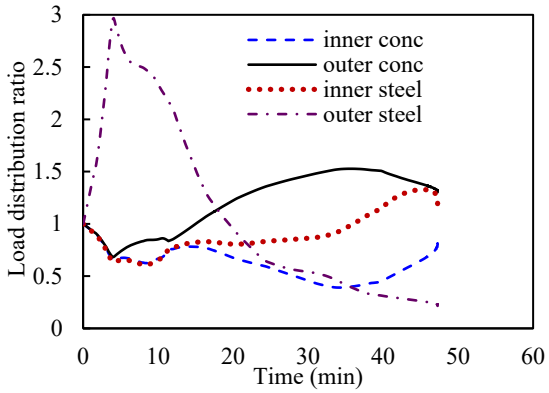

b) Ratio with applied load on each element at the beginning of fire condition

Fig. 7 load participation from different element

5.1. Effect of load level

The load level was changed by range from 0.1 to 0.7, as expected, increasing the load level decreases the fire resistance (FR) time and decreases the expansion of the column at the 1st phase. This is clearly indicated in Fig. 8.

5.2. Effect of inner width to thickness ratio

Fig. 9 shows the effect of the inner tube width to thickness (Di/ti) ratio, and it can be seen that increasing the Di/ti ratio leads to a decrease in FR time. Increasing the Di/ti ratio decreases the tube thickness, which makes to more vulnerable to local buckling. Besides, less thickness leads to high-temperature development in the inner steel tube.

5.3. Effect of outer width to thickness ratio

In contrary to the previous section, increasing the outer tube width-to-thickness (Do/to) ratio will lead to an increase in FR time. This is indicated in Fig. 10. Decreasing the Do/to ratio will increase the outer tube expansion of outer tube at the 1st phase. The load level was kept constant, so decreasing the Do/to ratio will decrease the load value. As the external tube fail in an earlier stage of the fire exposure, decreasing the Do/to ratio will lead to an increase in the FR time as a result of reducing load value.

5.4. Effect of steel tube strength

Fig. 11 shows the effect of steel tube strength (f_Y). Increasing steel tube strength decreases the FR time of CFDT columns. As mentioned before, in all columns, the load level was kept constant to a value of 0.4, so increasing f_Y will lead to an increase in the loading value on the column and as steel tubes (especially outer steel tubes) fail in an early stage of fire resistance this will increase the load on the inner and outer concrete and inner steel tube which will be responsible in carrying the whole applied load.

5.5. Effect of steel types

Four combinations were used to study the effect of steel tube types: inner and outer steel tube are stainless steel, inner and outer steel tubes are carbon steel, inner steel tube is stainless and outer is carbon and finally, inner steel tube is carbon and outer is stainless. In order to understand the difference in behavior been stainless steel and carbon steel under elevated temperatures, it's important to study their thermal and mechanical material properties, as illustrated in Figs. 12 and 13, respectively. As can be seen that stainless steel has less thermal conductivity and specific heat compared to carbon steel. However, carbon steel has a lower reduction strength factor compared to stainless steel up to nearly 600^{O}C. After that, the reduction factor of carbon steel began to be more than that of stainless steel. Fig. 14 shows that using stainless steel for the outer tube and carbon steel for the inner tube results in better behaviour. This is because steel at the outer tube provides slower temperature development through the column due to its material properties. While using carbon steel at the inner tube gains the benefit of carbon steel material properties, which has a lower reduction factor compared to stainless as, generally, the column fails when the inner tube temperature does not exceed 600 ^{O}C.

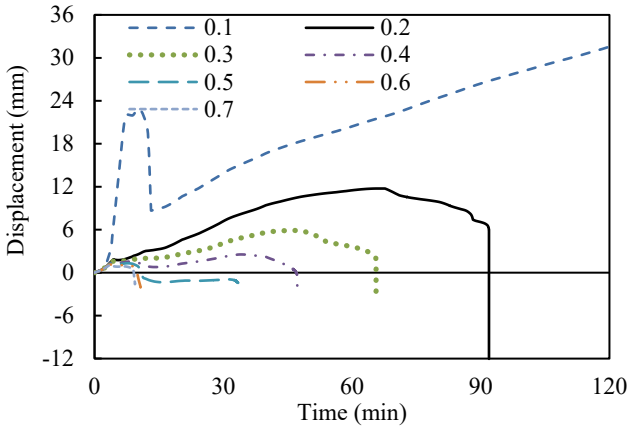

Fig. 8 Load level

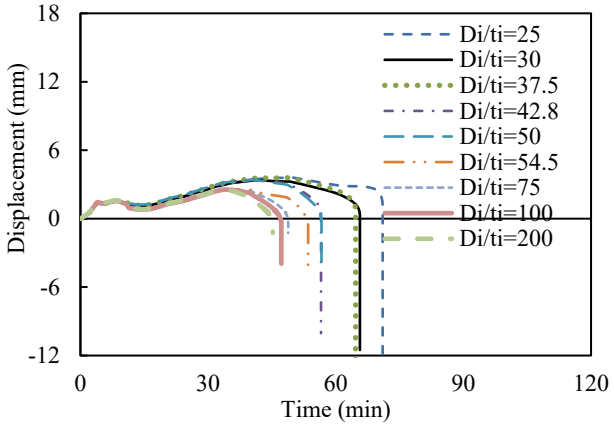

Fig. 9 Effect of inner width to thickness ratio

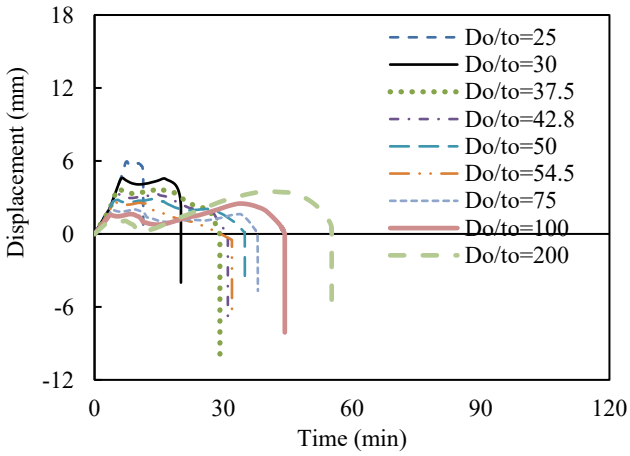

Fig. 10 Effect of outer width to thickness ratio

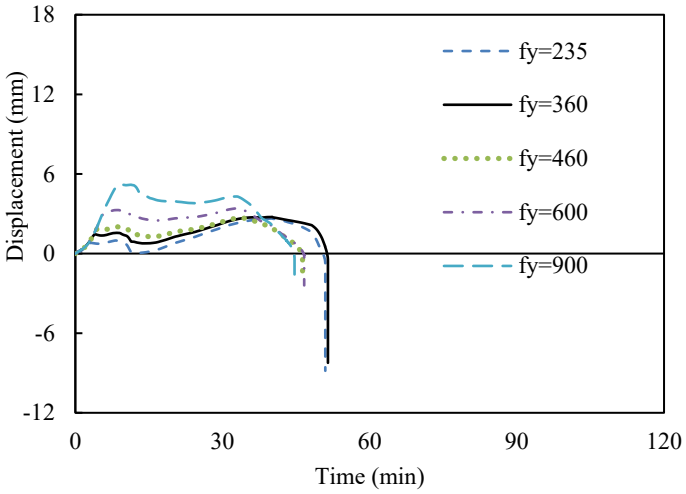

Fig. 11 Effect steel tube strength

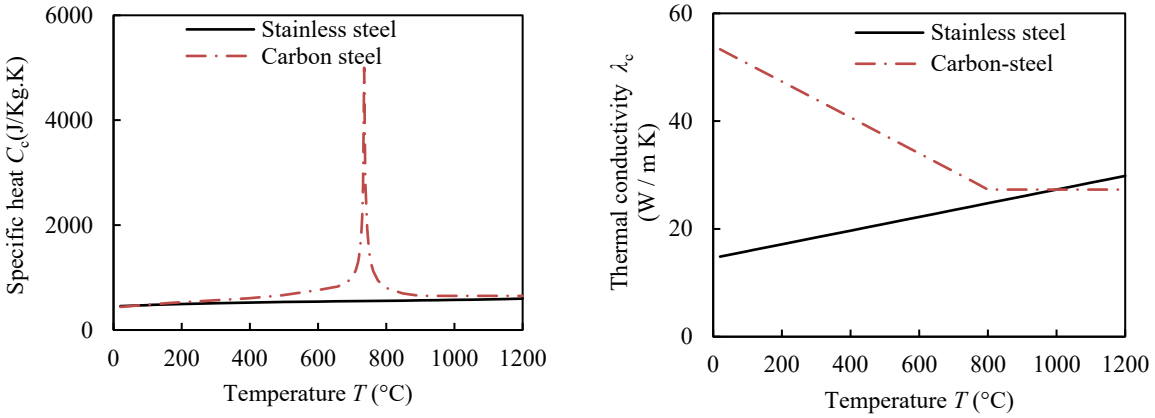

a) Specific heat

b) Thermal conductivity

Fig. 12 Thermal material properties of steel

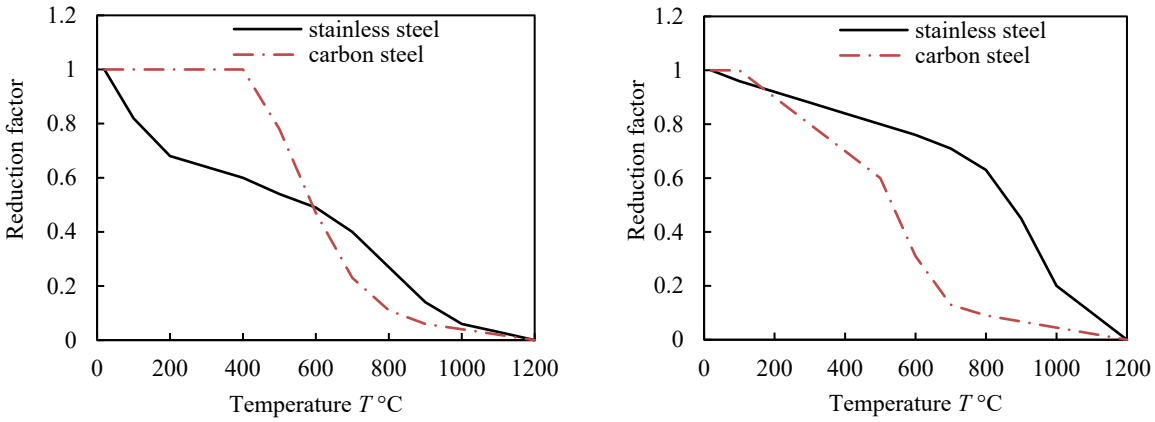

a) Yield strength

b) Elastic modulus

Fig. 13 mechanical material properties of steel

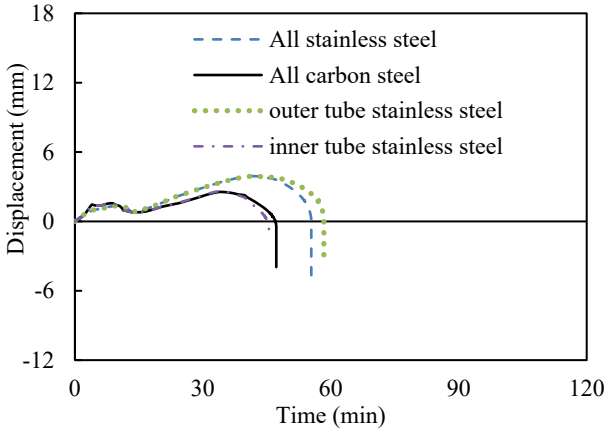

Fig. 14 Effect steel tube strength

5.6. Effect of inner-to-outer tube diameter ratio

The effect of inner to outer tube diameter (χ=Di/(Do-2to)) is shown in Fig. 15. Generally, it can be seen that increasing the ratio of inner to outer tube diameter will lead to an increase in the FR time. As mentioned before, the outer steel tube and outer concrete ring will carry most of the applied load at an early loading stage leaving the inner steel tube and inner concrete core to carry the load at a later stage. Increasing the inner tube diameter will increase the capacity of the inner steel tube and inner concrete core as a result of increasing its cross-sectional area, which in turn will increase the fire resistance time, especially at later stages of fire exposure.

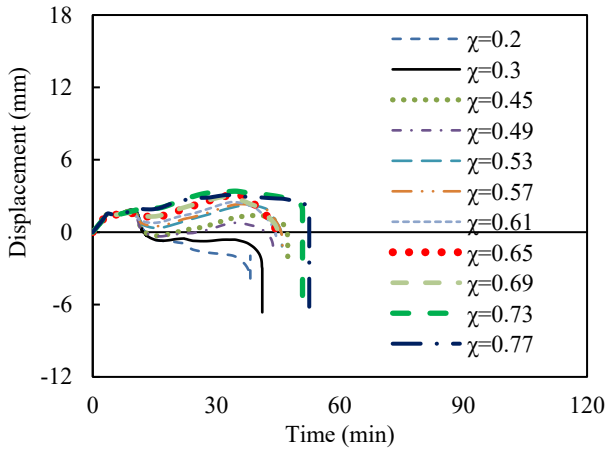

Fig. 15 Effect of inner to outer tube Diameter

5.7. Effect of slenderness ratio

The effect of column slenderness is shown in Fig. 16. It can be seen that the figure can generally be divided into three groups: 1st group from slenderness 24 to 80; in this stage, increasing column slenderness leads to an increase in FR time as a result of increasing flexural buckling. However, the 2nd group for slenderness, from 92 to 116, had a higher FR time than the slenderness group of 80. In the 2nd group, due to the larger column length, two actions opposite to each other take place. The first is flexural buckling, which tends to decrease the column flexural stiffens and thus the FR time. The second action is as a column length increases its expansion increases more, which takes a longer time to contract and therefore increases FR time. In the 2nd group, the second action overcomes the decrease in column flexural stiffness and, thus, the FR time increases.

The last and 3rd groups for the slenderness of 124, 136 and 144, the column length become larger and thus, the decrease in column flexural stiffness becomes more pronounced and therefore, the FR time decreases again.

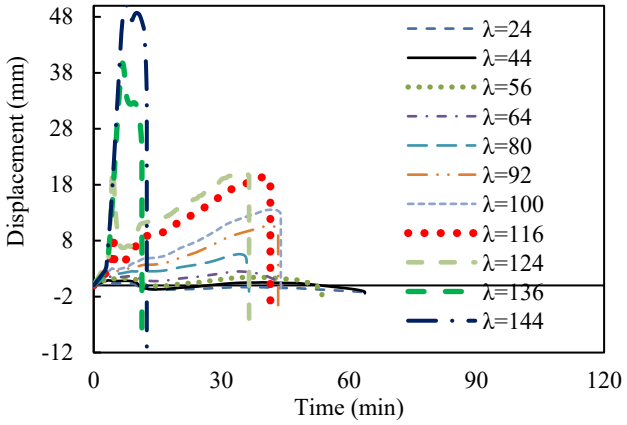

Fig. 16 Effect of column slenderness

5.8. Effect of concrete grade

As expected, increasing concrete compressive strength increases FR time, as indicated in Fig. 17 as the concrete ring and concrete core will be responsible for carrying the applied load after the outer and inner steel tube fails respectively as mentioned before.

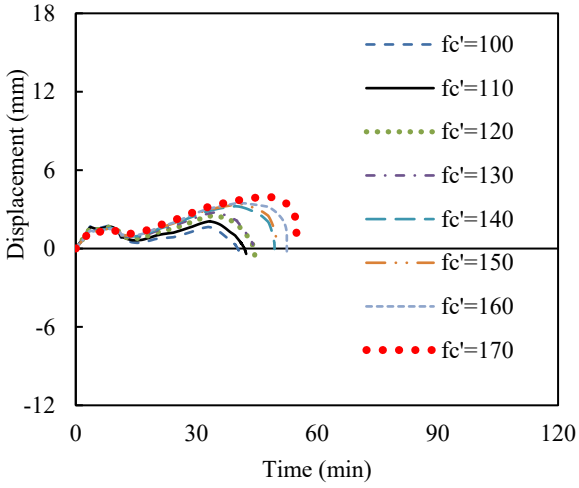

Fig. 17 Effect of concrete compressive strength

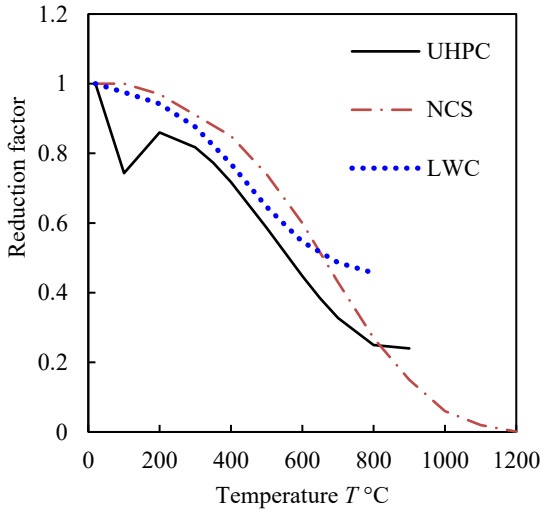

a) Compressive strength reduction factor

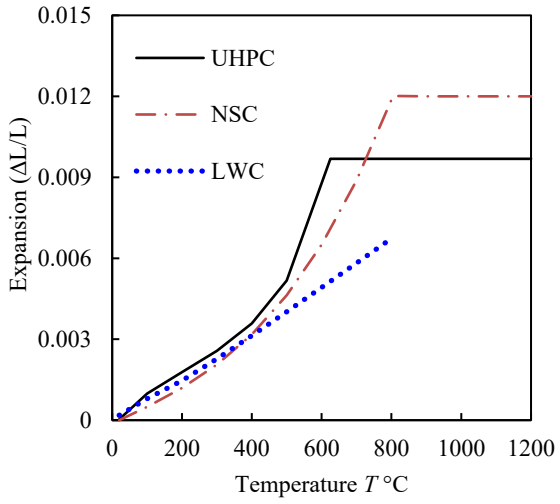

b) Expansion

Fig. 18 Mechanical material properties of concrete

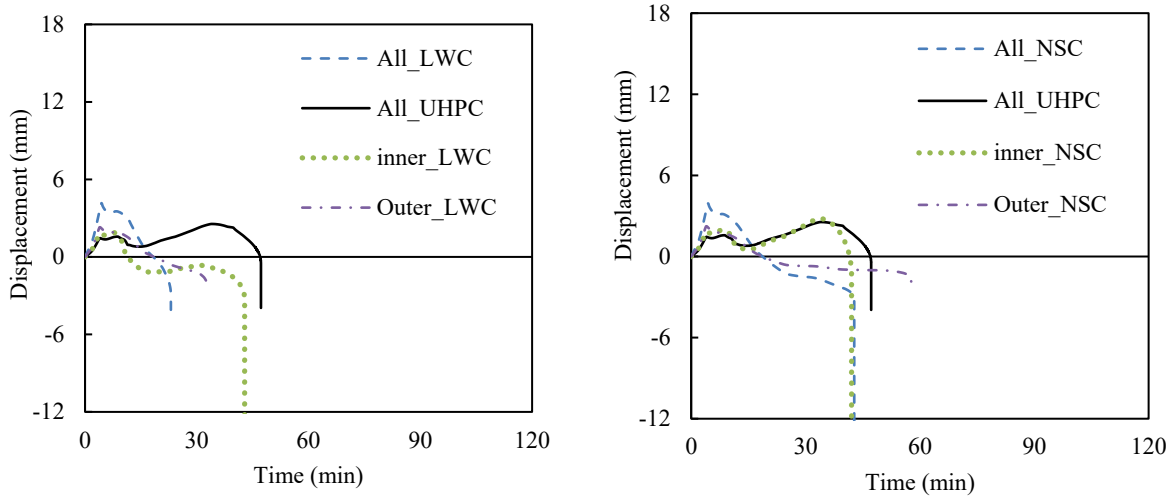

(a) LWC (b) NSC

Fig. 19 Effect of concrete type

5.9. Effect of concrete type

In this section, the effect of using different types of concrete, including Ultra high performance concrete (UHPC) normal strength concrete (NSC) and lightweight concrete (LWC) is investigated. Fig. 18 shows the effect in material properties between different types of concrete.

In Fig. 19a, four combinations were investigated: 1st LWC was used in the outer ring and in the inner core, 2nd combination UHPC was used in the outer ring and in the inner core, 3rd combination LWC was used in the inner concrete core and UHPC was used in the outer ring, while LWC was used in the outer ring and UHPC was used in inner core in the 4th combination.

It can be found that using UHPC in the outer ring and inner core gives higher FR time compared to other combinations. This is explained due to the closer reduction of the compressive strength factor between LWC and UHPC as indicated in Fig. 18a. However, UHPC has higher expansion compared to LWC, which gives UHPC more time to resist the applied force before material degradation and column failure.

In Fig. 19b, another four combinations were investigated using NSC: 1st NSC was used in the outer ring and in the inner core, 2nd combination UHPC was used in the outer ring and in the inner core, 3rd combination NSC was used in the inner concrete core and UHPC was used in the outer ring, while NSC was used in the outer ring and UHPC was used in inner core in the 4th combination. From Fig. 19b, it can be observed that using NSC at the outer ring and UHPC at the inner core give higher FR time. This is due to the lower reduction factor of NSC compared to UHPC as indicated in Fig. 18 (Unlike LWC's reduction factor is close to UHPC reduction factor), which results in decreasing the material degradation of the outer ring as it is exposed to higher temperature compared to inner core.

5.10. Effect of eccentricity

As illustrated in Fig. 20, eccentricity has a pronounced negative influence on the fire resistance of CFDST columns. The fire resistance decreased sharply from 47 minutes under concentric loading to 10 minutes when the eccentricity reached 0.1 of the column diameter. This reduction is primarily attributed to the combined effects of increased flexural demand induced by eccentric loading and the degradation of material properties at elevated temperatures, which accelerate the loss of column strength.

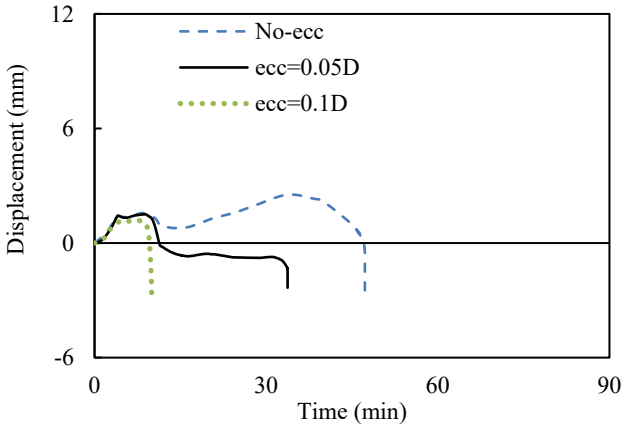

Fig. 20 Effect of Eccentricity

6. Evaluation of Eurocode 4

Eurocode 4 part 1.2 [25] is required the most widely accepted method in designing fire resistance of CFST columns under fire. In this section, an evaluation for Eurocode 4 part 1.2 [25] is performed using the results obtained from the parametric study. The evaluation is done through the comparison of the fire resistance (FR) time obtained from FE and from Eurocode; details are presented in the following sections.

6.1. Existing EC4 design approach

Eurocode 4 Part 1.2 provides a design model for evaluating the fire resistance of CFST columns. In this section, modifications to the Eurocode 4 model are proposed to extend its applicability to CFDT columns. The original EC4 Part 1.2 model is presented in Eq. 11.

$$N_{Rd,T} = \chi * N_{pl,Rd,T}$$

$N_{pl,Rd,T}$ is the cross-section capacity at elevated temperatures

$$N_{pl,Rd,T} = A_{\text{out,st,T}} \times f_{\text{out,st,y,T}} + A_{\text{out,c,T}} \times f_{\text{out,c,T}} + A_{\text{in,st,T}} \times f_{\text{in,st,y,T}} + A_{\text{in,c,T}} \times f_{\text{in,c,T}}$$

$$\chi = \frac{1}{\phi + \sqrt{\phi^2 - {\lambda_T}^2}} \qquad (11)$$

$$\phi = 0.5\,(1 + \alpha\,(\lambda_T - 0.2) + \lambda_T^2) \qquad \alpha = 0.49 \text{ related to buckling curve "c"}$$

where.

$$\lambda_T = \sqrt{N_{pl,R,T}\,/N_{cr,T}}$$

$$N_{cr,T} = \pi^2\,(E\,I)_{eff,T}\,/L^2$$

$$(E\,I)_{eff,T} = \varphi_{s,T}\,E_{s,T}\,I_s + \varphi_{c,T}\,E_{c,T}\,I_c + \varphi_{r,T}\,E_{r,T}\,I_r$$

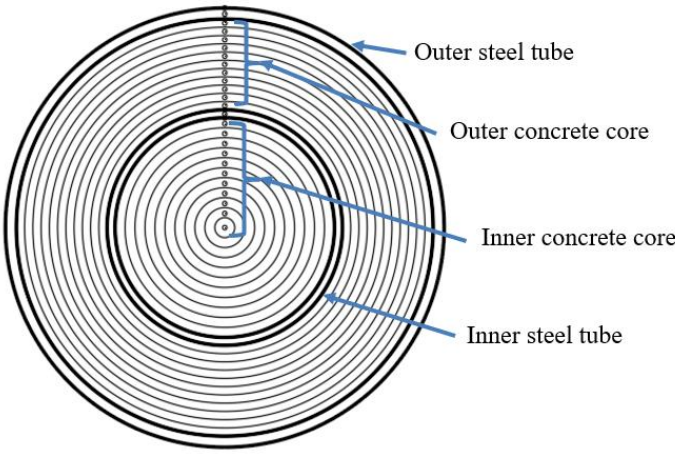

Fig. 21 Cross-section layers and divisions

6.2. Temperature development in CFDT columns

A finite difference (FD) model was developed using MATLAB to simulate the temperature distribution within CFDT columns. The formulation of this model is based on previous research by the authors for CFST and CFDST columns [58, 62]. The developed model predicts the temperature evolution at various locations across the cross-section, which is subsequently used to evaluate the temperature-dependent mechanical properties of the outer and inner steel tubes, as well as the outer and inner concrete regions.

The finite difference (FD) method was adopted in this study due to its simplicity, reduced computational cost, and shorter model-building time compared with the finite element (FE) approach [58, 62, 74]. To the authors' knowledge, no previous FD-based model has been developed for predicting the temperature distribution in CFDST columns; most available studies focus on CFST columns [62-64, 75], The authors have previously proposed a model for CFDST columns[58], and the present study extends this work by introducing an FD model to simulate temperature development through CFDST columns, thereby addressing this research gap.

In the proposed model, the cross-section was discretized into 11 layers for both the outer and inner concrete regions. The first and last layers in these regions were assigned half the thickness of the intermediate layers. For the inner and outer steel tubes, three layers were used, with the middle layer having twice the thickness of the first and last layers. The discretization scheme is illustrated in Fig. 21. To minimize accumulated numerical errors, the time step was selected as shown in the accompanying table.

Table 8
Time intervals (Δt) calculation

Time interval (Δ*t*) (sec)	Tube thickness (*t*) (mm)
0.03	$t \leq 3$
0.1	$3 < t \geq 5$
0.25	$5 < t \geq 7$
0.5	$7 < t \geq 12$
1	$t > 12$

The governing heat transfer equations, formulated based on [58, 62, 74], are presented in Equations [12-23].

For the outer surface of the steel tube:

$$T_{s1\_out}^{n+1} = T_{s1\_out}^{n} + \frac{\Delta t \times h_{total}}{\rho_{s1\_out}^{n} C_{s1\_out}^{n} \times \Delta x_{s1\_out}} - \frac{\Delta t}{\rho_{s1\_out}^{n} C_{s1\_out}^{n} \times \Delta x_{s1\_out} \times \left(\Delta x_{s1\_out} + \frac{\Delta x_{s2\_out}}{2}\right)} \times \left(\frac{K_{s1\_out}^{n} + K_{s2\_out}^{n}}{2}\right) \times \left(T_{s1\_out}^{n} - T_{s2\_out}^{n}\right) \quad (12)$$

where h_{total} (W/m^2) is the total heat energy from convection and radiation.

For the intermediate steel layer:

$$T_{s2\_out}^{n+1} = T_{s2\_out}^{n} + \frac{\Delta t}{\rho_{s2\_out}^{n} C_{s2\_out}^{n} \times \Delta x_{s2\_out} \times \left(\Delta x_{s1\_out} + \Delta x_{s2\_out}/2\right)} \times \left(\frac{K_{s1\_out}^{n} + K_{s2\_out}^{n}}{2}\right) \times \left(T_{s1\_out}^{n} - T_{s2\_out}^{n}\right) - \frac{\Delta t}{\rho_{s2\_out}^{n} C_{s2\_out}^{n} \times \Delta x_{s2\_out} \times \left(\Delta x_{s3\_out} + \Delta x_{s2\_out}/2\right)} \times \left(\frac{K_{s2\_out}^{n} + K_{s3\_out}^{n}}{2}\right) \times \left(T_{s2\_out}^{n} - T_{s3\_out}^{n}\right) \quad (13)$$

For the inner surface of the steel tube:

$$T_{s3\_out}^{n+1} = T_{s3\_out}^{n} + \frac{\Delta t}{\rho_{s3\_out}^{n} C_{s3\_out}^{n} \times \Delta x_{s3\_out} \times \left(\Delta x_{s3\_out} + \Delta x_{s2\_out}/2\right)} \times \left(\frac{K_{s2\_out}^{n} + K_{s3\_out}^{n}}{2}\right) \times \left(T_{s2\_out}^{n} - T_{s3\_out}^{n}\right) - \frac{\Delta t \times h_j}{\rho_{s3\_out}^{n} C_{s3\_out}^{n} \times \Delta x_{s3\_out}} \times \left(T_{s3\_out}^{n} - T_{c1\_out}^{n}\right) \quad (14)$$

For the outer concrete layer:

$$T_{c1\_out}^{n+1} = T_{c1\_out}^{n} \frac{\Delta t \times h_j}{\rho_{c1\_out}^{n} C_{c\_out}^{n} \times \Delta x_{c1\_out}} \times \left(T_{s3\_out}^{n} - T_{c1\_out}^{n}\right) - \frac{\Delta t}{\rho_{c1\_out}^{n} C_{c1\_out}^{n} \times \Delta x_{c1\_out} \times \left(\Delta x_{c1\_out} + \Delta x_{c2\_out}/2\right)} \times \left(\frac{K_{c1\_out}^{n} + K_{c2\_out}^{n}}{2}\right) \times \left(T_{c1\_out}^{n} - T_{c2\_out}^{n}\right) \quad (15)$$

For the intermediate concrete layer:

$$T_{cm\_out}^{n+1} = T_{cm\_out}^{n} + \frac{\Delta t}{\rho_{cm\_out}^{n} C_{cm\_out}^{n} \times \Delta x_{cm\_out} \times (\Delta x_{c(m-1)\_out}/2 + \Delta x_{cm\_out}/2)} \times \left(\frac{K_{c(m-1)\_out}^{n} + K_{cm\_out}^{n}}{2}\right) \times \left(T_{c(m-1)\_out}^{n} - T_{cm\_out}^{n}\right) - \frac{\Delta t}{\rho_{cm\_out}^{n} C_{cm\_out}^{n} \times \Delta x_{cm\_out} \times (\Delta x_{cm\_out}/2 + \Delta x_{c(m+1)\_out}/2)} \times \left(\frac{K_{cm\_out}^{n} + K_{c(m+1)\_out}^{n}}{2}\right) \times \left(T_{cm\_out}^{n} - T_{c(m+1)\_out}^{n}\right) \quad (16)$$

For the last concrete layer in the ring:

$$T_{cm\_out}^{n+1} = T_{cm\_out}^{n} + \frac{\Delta t}{\rho_{cm\_out}^{n} C_{cm\_out}^{n} \times \Delta x_{cm\_out} \times (\Delta x_{cm\_out} + \Delta x_{c(m-1)\_out})/2)} \times \left(\frac{K_{cm\_out}^{n} + K_{c(m-1)\_out}^{n}}{2}\right) \times \left(T_{c(m-1)\_out}^{n} - T_{cm\_out}^{n}\right) - \frac{\Delta t \times h_j}{\rho_{cm\_out}^{n} C_{cm\_out}^{n} \times \Delta x_{cm\_out}} \times \left(T_{cm\_out}^{n} - T_{s1\_in}^{n}\right) \quad (17)$$

For the outer steel layer of the inner tube:

$$T_{s1\_in}^{n+1} = T_{s1\_in}^{n} + \frac{\Delta t \times h_{j\_in}}{\rho_{s1\_in}^{n} C_{s1\_in}^{n} \times \Delta x_{s1\_in}} \times \left(T_{cm\_out}^{n} - T_{s1\_in}^{n}\right) - \frac{\Delta t}{\rho_{s1\_in}^{n} C_{s1\_in}^{n} \times \Delta x_{s1\_in} \times \left(\Delta x_{s1\_in} + \frac{\Delta x_{s2\_in}}{2}\right)} \times \left(\frac{K_{s1\_in}^{n} + K_{s2\_in}^{n}}{2}\right) \times \left(T_{s1\_in}^{n} - T_{s2\_in}^{n}\right) \quad (18)$$

For the intermediate steel layer:

$$T_{s2\_in}^{n+1} = T_{s2\_in}^{n} + \frac{\Delta t}{\rho_{s2\_in}^{n} C_{s2\_in}^{n} \times \Delta x_{s2\_in} \times (\Delta x_{s1\_in} + \Delta x_{s2\_in}/2)} \times \left(\frac{K_{s1\_in}^{n} + K_{s2\_in}^{n}}{2}\right) \times \left(T_{s1\_in}^{n} - T_{s2\_in}^{n}\right) - \frac{\Delta t}{\rho_{s2\_in}^{n} C_{s2\_in}^{n} \times \Delta x_{s2\_in} \times (\Delta x_{s3\_in} + \Delta x_{s2\_in}/2)} \times \left(\frac{K_{s2\_in}^{n} + K_{s3\_in}^{n}}{2}\right) \times \left(T_{s2\_in}^{n} - T_{s3\_in}^{n}\right) \quad (19)$$

For the inner surface of the steel tube:

$$T_{s3\_in}^{n+1} = T_{s3\_in}^{n} + \frac{\Delta t}{\rho_{s3\_in}^{n} C_{s3\_in}^{n} \times \Delta x_{s3\_in} \times (\Delta x_{s3\_in} + \Delta x_{s2\_in}/2)} \times \left(\frac{K_{s2\_in}^{n} + K_{s3\_in}^{n}}{2}\right) \times \left(T_{s2\_in}^{n} - T_{s3\_in}^{n}\right) - \frac{\Delta t \times h_{j\_in}}{\rho_{s3\_in}^{n} C_{s3\_in}^{n} \times \Delta x_{s3\_in}} \times \left(T_{s3\_in}^{n} - T_{c1\_in}^{n}\right) \quad (20)$$

For the outer concrete layer:

$$T_{c1\_in}^{n+1} = T_{c1\_in}^{n} \frac{\Delta t \times h_{j\_in}}{\rho_{c1\_in}^{n} C_{c1\_in}^{n} \times \Delta x_{c1\_in}} \times \left(T_{s3\_in}^{n} - T_{c1\_in}^{n}\right) - \frac{\Delta t}{\rho_{c1\_in}^{n} C_{c1\_in}^{n} \times \Delta x_{c1\_in} \times (\Delta x_{c1\_in} + \Delta x_{c2\_in}/2)} \times \left(\frac{K_{c1\_in}^{n} + K_{c2\_in}^{n}}{2}\right) \times \left(T_{c1\_in}^{n} - T_{c2\_in}^{n}\right) \quad (21)$$

For the intermediate concrete layer:

$$T_{cm\_in}^{n+1} = T_{cm\_in}^{n} + \frac{\Delta t}{\rho_{cm\_in}^{n} C_{cm\_in}^{n} \times \Delta x_{cm\_in} \times (\Delta x_{c(m-1)\_in}/2 + \Delta x_{cm\_in}/2)} \times \left(\frac{K_{c(m-1)\_in}^{n} + K_{cm\_in}^{n}}{2}\right) \times \left(T_{c(m-1)\_in}^{n} - T_{cm\_in}^{n}\right) - \frac{\Delta t}{\rho_{cm\_in}^{n} C_{cm\_in}^{n} \times \Delta x_{cm\_in} \times (\Delta x_{cm\_in}/2 + \Delta x_{c(m+1)\_in}/2)} \times \left(\frac{K_{cm\_in}^{n} + K_{c(m+1)\_in}^{n}}{2}\right) \times \left(T_{cm\_in}^{n} - T_{c(m+1)}\right) \quad (22)$$

For the last concrete layer in the ring:

$$T_{cm\_in}^{n+1} = T_{cm\_in}^{n} + \frac{\Delta t \times 2}{\rho_{cm\_in}^{n} c_{cm\_in}^{n} \times \Delta x_{cm\_in} \times (\Delta x_{c(m-1)\_in}/2 + \Delta x_{cm\_in})} \times \left(\frac{K_{c(m-1)\_in}^{j} + K_{cm\_in}^{j}}{2}\right) \times \left(T_{c(m-1)\_in}^{j} - T_{cm\_in}^{j}\right) \quad (23)$$

where the superscript *n* denotes the time step in seconds; cm refers to the layer number *m* in the concrete core; the subscript sm rrefers to the layer number *m* in the steel tube; the subscript _out denotes the outer tube or outer core, while the subscript _in denotes the inner tube or inner core. *T* represents the temperature (°C); *d* is the distance from the outer surface of the considered layer to the column center (m); Δx is the layer thickness (m); Δt is the time interval (s); *C* is the specific heat capacity ($J/kg \cdot K$); ρ is the material density (kg/m^3); *K* is the thermal conductivity (W/m·K); α_c is the convective heat transfer coefficient; and h_j is the thermal conductance between the steel tube and the concrete (W/m^2K).

Fig. 22 shows the validation of the proposed analytical model (AM) against the finite element (FE) results at multiple points across the CFDST cross-section. A good agreement was achieved between the two models in terms of temperature prediction. The verification was performed on a column with an outer steel tube of 500 mm diameter and 5 mm thickness, and an inner steel tube of 300 mm diameter and 3 mm thickness. The concrete infill consisted of ultra-high-performance concrete (UHPC) with a compressive strength of 120 MPa, while both steel tubes had a yield strength of 360 MPa.

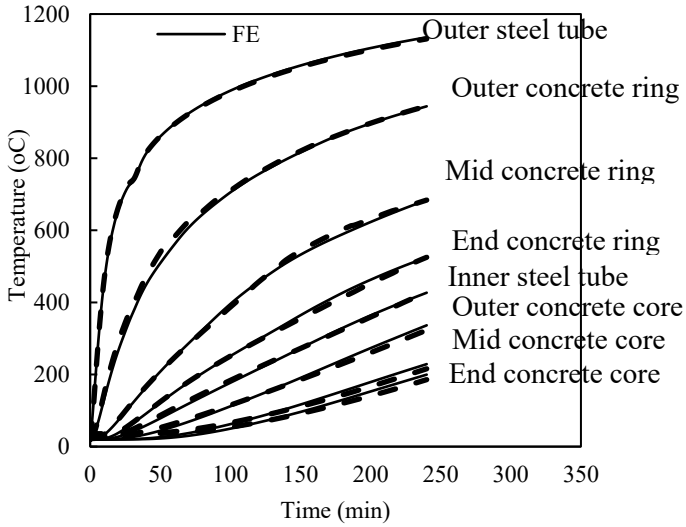

Fig. 22 Verification of FD model

6.3. Proposed buckling curve modification

This section presents a comparative analysis of fire resistance (FR) times predicted by Eurocode 4 (EC4), implemented through a MATLAB-based analytical model, against those obtained from a validated finite element (FE) model. In the corresponding figure, the X-axis represents the FR time predicted by the FE model, while the Y-axis shows the FR time estimated using both the original and the modified EC4 formulations.

The results indicate that the standard EC4 substantially underestimates the fire resistance of CFDT columns incorporating ultra-high-performance concrete (UHPC). To improve prediction accuracy, a modification to the EC4 buckling curve was proposed. Based on regression analysis, the buckling curve factor (α) was adjusted to 0.85.

The applicability of the proposed buckling curve is limited to the following parameter ranges: load level from 0.1 to 0.7; inner tube diameter-to-thickness ratio between 25 and 200; outer tube diameter-to-thickness ratio between 25 and 200; inner-to-outer tube diameter ratio from 0.2 to 0.77; steel yield strength between 235 and 900 MPa; concrete cylinder strength between 100 and 170 MPa; and slenderness ratio from 25 to 144.

As shown in Fig. 23, the modified EC4 model yields predictions that align more closely with the FE results. Table 9 summarizes the comparative performance: the average test-to-prediction ratio improved from 1.464 (original EC4) to 0.992 (modified EC4), while the coefficient of variation (COV) was reduced from 0.311 to 0.298.

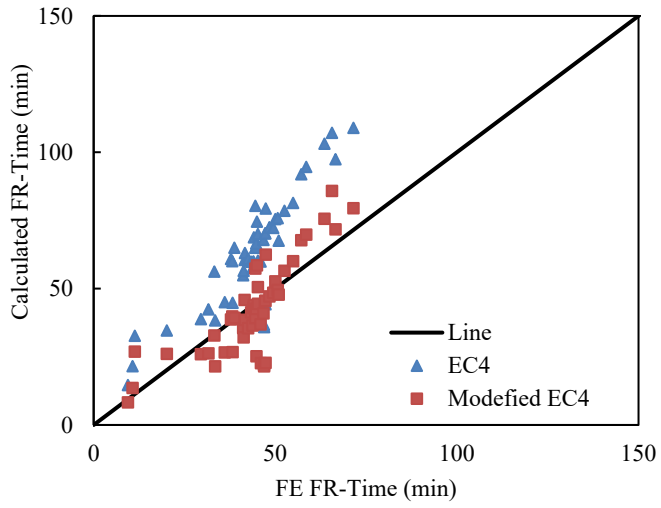

Fig. 23 Evaluation f EC4 1.2

Table 9
Comparison between EC4 and modified model

	EC4	Modified EC4
Mean	1.464	0.992
COV	0.311	0.298

7. Conclusions

This paper presents an analytical and numerical investigation aimed at enhancing the understanding of ultra-high-performance concrete-filled double-skin tubular (UHPC-CFDT) columns under fire conditions and addressing the existing research gap in this field. Based on available experimental data, three temperature-dependent material models were developed to simulate the behavior of UHPC, lightweight concrete, and high-strength steel at elevated temperatures.

A validated finite element (FE) model was developed, showing strong agreement with existing test results. Additionally, an automated Python-based FE modeling framework was established, enabling efficient model generation, analysis execution, and data extraction. This tool is particularly valuable for engineers with limited experience in Abaqus and for expediting extensive parametric studies.

Based on the parametric investigations conducted and the proposed models, the following conclusions and recommendations can be drawn:

- Fire resistance increases with the outer tube diameter-to-thickness ratio (Do/to), the inner-to-outer tube diameter ratio, and the concrete compressive strength. For example, fire resistance increased from 11 to 55 minutes as the Do/to ratio rose from 25 to 200.
- In contrast, fire resistance decreases with higher load levels, inner tube diameter-to-thickness ratio, and steel yield strength. Among these, load level had the most pronounced effect, with fire resistance increasing nearly tenfold as the load level decreased from 0.7 to 0.2.
- The optimal material configuration under fire conditions was identified as stainless steel for the outer tube, carbon steel for the inner tube, normal-strength concrete in the outer ring, and UHPC in the inner core.
- A finite difference model was developed to accurately simulate temperature distribution across the cross-section of UHPC-filled CFDT columns during fire exposure.
- The Eurocode 4 (EC4) design approach was evaluated against the FE results. It was found that EC4 provides unconservative predictions for the fire resistance of UHPC-filled CFDT columns. A simplified modification is proposed by adjusting the buckling curve factor (α) to 0.85, thereby improving the accuracy of the nominal resistance prediction under fire.

In conclusion, this study focused on circular CFDT columns exposed to fire. Further research is recommended to investigate the fire behavior of UHPC-filled CFDT columns with square, octagonal, or hexagonal cross-sections and various geometric and material configurations.

References

[1] Le TT, Patel VI, Liang QQ, Huynh P. Numerical modeling of rectangular concrete-filled double-skin steel tubular columns with outer stainless-steel skin. Journal of Constructional Steel Research. 2021;179:106504.

[2] Romero ML, Espinos A, Portolés JM, Hospitaler A, Ibañez C. Slender double-tube ultra-high strength concrete-filled tubular columns under ambient temperature and fire. Engineering Structures. 2015;99:536-45.

[3] Tao Z, Han L-H, Zhao X-L. Behaviour of concrete-filled double skin (CHS inner and CHS outer) steel tubular stub columns and beam-columns. Journal of Constructional Steel Research. 2004;60:1129-58.

[4] Tao Z, Han L-H. Behaviour of concrete-filled double skin rectangular steel tubular beam–columns. Journal of Constructional Steel Research. 2006;62:631-46.

[5] Han L-H, Huang H, Tao Z, Zhao X-L. Concrete-filled double skin steel tubular (CFDST) beam–columns subjected to cyclic bending. Engineering Structures. 2006;28:1698-714.

[6] Mohan AP, S A. Non-Linear Analysis of Concrete Filled Double Skin Circular Steel Column. International Journal of Engineering Research & Technology (IJERT). 2016;5:204-6.

[7] Elchalakani M, Hassanein MF, Karrech A, Yang B. Experimental investigation of rubberised concrete-filled double skin square tubular columns under axial compression. Engineering Structures. 2018;171:730-46.

[8] Hassanein MF, Elchalakani M, Karrech A, Patel VI, Daher E. Finite element modelling of concrete-filled double-skin short compression members with CHS outer and SHS inner tubes. Marine Structures. 2018;61:85-99.

[9] Ghannam M, Metwally IM. Numerical investigation for the behaviour of stiffened circular concrete filled double tube columns. Structures. 2020;25:901-19.

[10] Karthika S, Ranjitham M. Study of Strength and Behaviour of Concrete Filled Double Skin Tubular Square Columns under Axial Compressive Loads. International Journal of Engineering Research & Technology (IJERT). 2016;5:746-51.

[11] Huang H, Han L-H, Tao Z, Zhao X-L. Analytical behaviour of concrete-filled double skin steel tubular (CFDST) stub columns. Journal of Constructional Steel Research. 2010;66:542-55.

[12] Ekmekyapar T, Al-Eliwi BJM. Concrete filled double circular steel tube (CFDCST) stub columns. Engineering Structures. 2017;135:68-80.

[13] Jia-qi -L, Rui -W, Hui -Z, Hui-wen -W. - STUDY ON THE FIRE PERFORMANCE OF CONCRETE-FILLED DOUBLE-SKIN TUBULAR COLUMNS WITH EXTERNAL STAINLESS STEEL TUBES. - Engineering Mechanics. 2020;- 37:- 125.

[14] Lopes RFR, Rodrigues JPC. Behaviour of restrained concrete filled square double-skin and double-tube hollow columns in case of fire. Engineering Structures. 2020;216:110736.

[15] Lu H, Zhao X-L, Han L-H. FE modelling and fire resistance design of concrete filled double skin tubular columns. Journal of Constructional Steel Research - J CONSTR STEEL RES. 2011;67:1733-48.

[16] Xiong M. Fire resistance of ultra-high strength concrete filled steel tubular columns: PhD Dissertation, National University of Singapore, Singapore; 2013.

[17] Wan C-Y, Zha X-X, Dassekpo J-BM. Analysis of axially loaded concrete filled circular hollow double steel tubular columns exposed to fire. Fire Safety Journal. 2017;88:1-12.

[18] Imani R, Bruneau M, Mosqueda G. Simplified analytical solution for axial load capacity of concrete-filled double-skin tube (CFDST) columns subjected to fire. Engineering Structures. 2015;102:156-75.

[19] Zhu H, Ahmed M, Li C, Kong X, Chen S, Yang Q et al. Fire resistance of square double-skin concrete-filled steel tubular columns and concrete-filled double steel tubular columns. Engineering Structures. 2024;319:118882.

[20] Zhu H, Chen S, Ahmed M, Liang QQ. Experimental and numerical investigations of circular concrete filled steel double-skin and double-tube columns exposed to fire. Thin-Walled Structures. 2024;198:111766.

[21] Zhu H, Chen S, Ahmed M, Li C, Kong X, Ghazali H et al. Behavior and design of eccentrically loaded circular concrete-filled double steel tubular beam-columns under fire exposure. Thin-Walled Structures. 2025;208:112806.

[22] Yao Y, Li H, Tan K-H. Theoretical and numerical analysis to concrete filled double skin steel tubular columns under fire conditions. Thin-Walled Structures. 2016;98:547-57.

[23] Yao Y, Liu M, Guo H. Concrete filled double skin steel tubular columns subjected to non-uniform heating. Journal of Constructional Steel Research. 2019;158:263-78.

[24] Shekastehband B, Taromi A, Abedi K. Fire performance of stiffened concrete filled double skin steel tubular columns. Fire Safety Journal. 2017;88:13-25.

[25] Eurocode-4. Design of composite steel and concrete structures, part 1.2 General rules, Structural fire design. London: BS EN 1994-1-2:2005. British Standards Institution; 2005.

[26] Shen P, Lu J-X, Zheng H, Lu L, Wang F, He Y et al. Expansive ultra-high performance concrete for concrete-filled steel tube applications. Cement and Concrete Composites. 2020;114:103813.

[27] Liu K, Wu C, Li X, Liu J, Tao M, Fang J et al. The influences of cooling regimes on fire resistance of ultra-high performance concrete under static-dynamic coupled loads. Journal of Building Engineering. 2021:103336.

[28] Zhang D, Liu Y, Tan KH. Spalling resistance and mechanical properties of strain-hardening ultra-high performance concrete at elevated temperature. Construction and Building Materials. 2021;266:120961.

[29] Li Y, Du P, Tan KH. Fire resistance of ultra-high performance concrete columns subjected to axial and eccentric loading. Engineering Structures. 2021;248:113158.

[30] Lyzwa J, Zehfuss J. Experimental Investigations of ultra-high performance concrete exposed to natural fires. Fire Safety Journal. 2021:103399.

[31] Banerji S, Kodur V. Effect of temperature on mechanical properties of ultra-high performance concrete. Fire and Materials. 2021.

[32] Li Y. Effect of post-fire curing and silica fume on permeability of ultra-high performance concrete. Construction and Building Materials. 2021;290:123175.

[33] Mai V-C, Nguyen T-C, Dao C-B. Numerical simulation of ultra-high-performance fiber-reinforced concrete frame structure under fire action. Asian Journal of Civil Engineering. 2020:1-8.

[34] Du Y, Qi H-H, Huang S-S, Liew JR. Experimental study on the spalling behaviour of ultra-high strength concrete in fire. Construction and Building Materials. 2020;258:120334.

[35] Xiong M-X, Liew JR. Mechanical behaviour of ultra-high strength concrete at elevated temperatures and fire resistance of ultra-high strength concrete filled steel tubes. Materials & Design. 2016;104:414-27.

[36] Banerji S, Kodur V, Solhmirzaei R. Experimental behavior of ultra high performance fiber reinforced concrete beams under fire conditions. Engineering Structures. 2020;208:110316.

[37] Chen H-J, Yu Y-L, Tang C-W. Mechanical properties of ultra-high performance concrete before and after exposure to high temperatures. Materials. 2020;13:770.

[38] Xiong M-X, Liew JR. Buckling behavior of circular steel tubes infilled with C170/185 ultra-high-strength concrete under fire. Engineering Structures. 2020;212:110523.

[39] Xiong M-X, Liew JR. Fire resistance of high-strength steel tubes infilled with ultra-high-strength concrete under compression. Journal of Constructional Steel Research. 2021;176:106410.

[40] Wang T, Yu M, Zhang X, Xu L, Huang L. Experimental study and proposal of a design model of ultra-high performance concrete filled steel tube columns subjected to fire. Engineering Structures. 2023;280:115697.

[41] Camargo AL, Rodrigues JPC, Fakury RH, Laim L. Fire Resistance of Axially and Rotationally Restrained Concrete-Filled Double-Skin and Double-Tube Hollow Steel Columns. Journal of Structural Engineering. 2019;145:04019128.

[42] Lee YW, Kim GY, Gucunski N, Choe GC, Yoon MH. Thermal strain behavior and strength degradation of ultra-high-strength-concrete. Materials and structures. 2016;49:3411-21.

[43] Choe G, Kim G, Gucunski N, Lee S. Evaluation of the mechanical properties of 200 MPa ultra-high-strength concrete at elevated temperatures and residual strength of column. Construction and Building Materials. 2015;86:159-68.

[44] Khaliq W. Mechanical and physical response of recycled aggregates high-strength concrete at elevated temperatures. Fire safety journal. 2018;96:203-14.

[45] Cheng F-P, Kodur V, Wang T-C. Stress-strain curves for high strength concrete at elevated temperatures. Journal of Materials in Civil Engineering. 2004;16:84-90.

[46] Phan LT, Carino NJ. Effects of test conditions and mixture proportions on behavior of high-strength concrete exposed to high temperatures. ACI Materials Journal. 2002;99:54-66.

[47] Chen J, Young B, Uy B. Behavior of high strength structural steel at elevated temperatures. Journal of structural engineering. 2006;132:1948-54.

[48] Lange J, Wohlfeil N. Examination of the mechanical properties of steel S460 for fire. Journal of Structural Fire Engineering. 2010.

[49] Qiang X, Bijlaard F, Kolstein H. Dependence of mechanical properties of high strength steel S690 on elevated temperatures. Construction and Building Materials. 2012;30:73-9.

[50] Qiang X, Bijlaard FS, Kolstein H. Deterioration of mechanical properties of high strength structural steel S460N under steady state fire condition. Materials & Design (1980-2015). 2012;36:438-42.

[51] Choi I-R, Chung K-S, Kim D-H. Thermal and mechanical properties of high-strength structural steel HSA800 at elevated temperatures. Materials & Design. 2014;63:544-51.

[52] Heidarpour A, Tofts NS, Korayem AH, Zhao X-L, Hutchinson CR. Mechanical properties of very high strength steel at elevated temperatures. Fire safety journal. 2014;64:27-35.

[53] Wang W, Zhang Y, Xu L, Li X. Mechanical properties of high-strength Q960 steel at elevated temperature. Fire Safety Journal. 2020;114:103010.

[54] Li G-Q, Song L-X. Mechanical properties of TMCP Q690 high strength structural steel at elevated temperatures. Fire Safety Journal. 2020;116:103190.

[55] Lu H, Han L-H, Zhao X-L. Fire performance of self-consolidating concrete filled double skin steel tubular columns: Experiments. Fire Safety Journal. 2010;45:106-15.

[56] Mohd Zuki SS, Shahidan S, Choong K, Jayaprakash J, Ali N. Concrete-Filled Double Skin Steel Tubular Columns Exposed to ASTM E-119 Fire Curve for 60 and 90 Minutes of Fire. MATEC Web of Conferences. 2017;103:02009.

[57] ABAQUS. ABAQUS standard user's manual, Version 6.14. USA: Dassault Systèmes Corp., Providence, RI; 2014.

[58] Abdelrahman AHA, Ghannam M, Lotfy S, AlHamaydeh M. Heat Transfer in Ultra-High-Performance Concrete-Filled Double-Skin Tubes Under Fire Conditions. Fire Technology. 2023;59:1519-54.

[59] Eurocode-3. Part 1-2 Design of steel structures, Part 1-2, General rules, structural fire design. BS EN 1993-1-2:2005. British Standards Institution, London; 2005.

[60] Liu X, Liu Z, Hui Y, Wang J. Research on the Concrete-Filled Double Skin steel Tubular (CFDST) columns subjected to axial force after fire. Structures. 2023;57:105213.

[61] Eurocode-2. Design of concrete structures, Part 1-2, General rules, structural fire design. London: BS EN 1992-1-2:2004, British Standards Institution; 2005.

[62] Ghannam M, Song TY. Fire Resistance Design of Concrete-Filled Steel Tube Stub Columns. Fire Technology. 2021;57:911-42.

[63] Xiong M-X, Liew JYR. Buckling behavior of circular steel tubes infilled with C170/185 ultra-high-strength concrete under fire. Engineering Structures. 2020;212:110523.

[64] Lie T, Irwin R. Fire resistance of rectangular steel columns filled with bar-reinforced concrete. Journal of Structural Engineering. 1995;121:797-805.

[65] Baloch WL, Khushnood RA, Memon SA, Ahmed W, Ahmad S. Effect of Elevated Temperatures on Mechanical Performance of Normal and Lightweight Concretes Reinforced with Carbon Nanotubes. Fire Technology. 2018;54:1331-67.

[66] Albozagre H, Naghipour M. Experimental study of the behaviour of the concrete-filled double-skin columns with stainless-steel outer tubes subjected to post-earthquake fire. Structures. 2025;75:108541.

[67] ACI216R-89. Guide for Determining the Fire Endurance of Concrete Elements. American Concrete Institute. 1994.

[68] AISC. Specification for Structural Steel Buildings. Standard ANSI/AISC 360-16. United States of America: American Institute of Steel Construction, Inc; 2016.

[69] AS/NZS_2327. composite structures composite steel-concrete construction in building. Sydney, Australia: Australian Standard/New Zealand Standard, Standards Australia; 2017.

[70] ASCE. Structural fire protection. Manual No. 78. ASCE Committee on Fire Protection, Structural Division, American Society of Civil Engineers, New York, USA. 1992.

[71] Ci J, Ahmed M, Liang QQ, Chen S, Chen W, Sennah K et al. Experimental and numerical investigations into the behavior of circular concrete-filled double steel tubular slender columns. Engineering Structures. 2022;267:114644.

[72] Xiong M-X, Xiong D-X, Liew JYR. Behaviour of steel tubular members infilled with ultra high strength concrete. Journal of Constructional Steel Research. 2017;138:168-83.

[73] ISO-834-1. Fire-resistance tests-Elements of building construction-Part 1: General requirements. Geneva: International Organization for Standardization; 1999.

[74] Harmathy T. Fire safety design and concrete. United Kingdom,: Longman Scientific and technical; 1993.

[75] Lie TT, Chabot M. A method to predict the fire resistance of circular concrete filled hollow steel columns. Journal of Fire Protection Engineering. 1990;2:111-24.